Available online at www.sciencedirect.com
ScienceDirect
Polymer 48 (2007) 3148–3161
polymer
www.elsevier.com/locate/polymer

Temperature-induced structural changes in some random ethylene/1-hexene copolymers

Kenneth D. Knudsen [a,*], Pål V. Hemmingsen [b], Frode Mo [c]

[a] Department of Physics, Institute for Energy Technology, P.O. Box 40, N-2027 Kjeller, Norway
[b] Department of Chemical Engineering, Norwegian University of Science and Technology, N-7491 Trondheim, Norway
[c] Department of Physics, Norwegian University of Science and Technology, N-7491 Trondheim, Norway

Received 12 December 2006; received in revised form 19 March 2007; accepted 25 March 2007
Available online 3 April 2007

Abstract

Powder diffraction measurements on five unoriented samples of poly(ethylene-*co*-hexene) were performed in the temperature range 23–200 °C using synchrotron X-radiation in combination with an area detector. Melting and recrystallization was found to improve the crystallinity of the samples, resulting in a denser packing along [010] or *b* for the most crystalline samples. A high content of cohexene (branching) reduces both the melting temperature T_m and the crystallinity. There appears to be a slight increase in T_m with increasing molecular weight M_n of the sample. The coefficient of thermal expansion (CTE) along [100], α_a, was found to be always positive, in the range $(26–34) \times 10^{-5}$ K^{-1} up to melting, with the larger values for the most crystalline samples. The CTE in the chain direction, *i.e.* α_c along [001], is negative, ranging from $(-0.6$ to $-8.0) \times 10^{-5}$ K^{-1}. The thermal response in the [010] direction is more complex, in most cases being significantly different in the heating and cooling sequences. The unit cells expand nearly linearly in the temperature range from RT to about 20 °C below T_m. Increasing T towards T_m brings about an enhanced asymmetry in the C–C–H valency angles and a small rotation of the polymer chains with a concomitant expansion of the interchain contacts lying approximately in the *bc*-plane. Melting and recrystallization induce a shortening of these contacts and both the atomic and the molecular movements involved in the structural changes are reversed during cooling.

Keywords: Poly(ethylene-*co*-hexenes); Thermal effects on structure; Synchrotron X-ray diffraction

1. Introduction

Copolymerization of ethylene with an α-olefin monomer will introduce branches in the highly regular polyethylene backbone, and thereby influence its basic structure as well as a range of thermal, mechanical and optical properties. The macroscopic properties are not easily predictable from a theoretical point of view, but based on empirical knowledge the processing conditions can be tuned to yield a polymer with specific and desired characteristics. The macroscopic properties depend mainly on a few factors: in addition to molecular weight and the crystallization and annealing conditions, also on the concentration, regularity and size of the short-chain branches along the main polymer chain. Weight-average molecular weights of commercial polyethylenes are typically in the range from about 2000 to 3000 g mol^{-1} (low M_w PE) to more than 5,000,000 g mol^{-1} (ultra high M_w PE), representing a wide range in overall chain length. Polyethylenes are prepared by different techniques. Low-density polyethylenes (LDPE) are produced by autoclave or tubular reactor technology at high pressure. This gives a polymer with a high content of long-chain branching, low crystallinity and hence low density. High-density polyethylenes (HDPE) are polymerized in a low pressure slurry, in solution or gas-phase reactors. By the use of various catalysts with distinct properties, comonomers like butene, hexene or octene can be incorporated into the main polymer chain as short branches for the purpose of controlling the density of the resulting polymer. Linear

* Corresponding author. Tel.: +47 63806084; fax: +47 63810920.
E-mail address: knudsen@ife.no (K.D. Knudsen).

0032-3861/$ - see front matter © 2007 Elsevier Ltd. All rights reserved.
doi:10.1016/j.polymer.2007.03.060

low-density polyethylene (LLDPE) is produced in this manner by increasing the content of short-chain branches. The M_w and its distribution (polydispersity) together with the comonomer size and content of branching will finally affect the optimal packing of the chains into microcrystallites, the amount of free chain segments extending out from the microcrystallites, and the relative amount of non-crystalline and crystalline fractions of the final material. These factors, together with the thermal and mechanical processing parameters, determine effectively the polymer properties that are important for the application of a certain type of polyethylene.

As a means of gaining information about the microstructural changes taking place in the crystalline part of a semi-crystalline material when an external parameter, *e.g.* temperature, is changed, one may study the thermally induced changes of the crystal lattice, including melting and recrystallization. The Rietveld method [1,2] applied to powder diffractograms is a very accurate method for determination of lattice constants, due to the large number of precisely located diffraction peaks that can be introduced in the whole-pattern fit, thereby contributing to small standard deviations in the computed lattice constants. A modern two-dimensional electronic detector in combination with the high-flux and low-divergent X-rays from a synchrotron source, provide a very efficient tool for structural characterization of polycrystalline materials. The quality of the sample may be the limiting factor for the usefulness of this procedure, as samples with low crystallinity will have inherently broadened diffraction peaks. However, the resolution in the diffraction spectrum for any given sample, will be superior to that obtained with a standard laboratory X-ray source because of the smaller flux and generally much larger divergence of that beam. We show in the present paper that the combination of an image-plate detector and synchrotron X-rays may give high quality patterns of polyethylenes with well-resolved diffraction peaks down to *d*-values of about 1.25 Å in less than 1 min, thus enabling a detailed study of the effect of temperature on these samples. This method also opens for time-resolved studies of the impact of other external parameters, such as pressure, tension, radiation or fields.

2. Experimental

2.1. Materials

The ethylene copolymer samples used in this work were provided by Borealis AS. They were synthesised in a low-pressure slurry process using isobutane as solvent, and different amounts of the comonomer 1-hexene were incorporated into the chains. The powder samples were taken from the reactor as untreated granular material.

2.2. X-ray diffraction study

The largest particles were removed using a sieve of mesh size 60, giving particles of size less than 250 μm. The samples were filled in 1.5 mm borosilicate capillaries and mounted in 8 mm brass stubs, with inner diameter 1.7 mm. The brass stub was subsequently inserted into a Huber goniometer head (1005), which was mounted on the spindle axis of a MAR345 image-plate system. The distance between the sample and detector was chosen to be nominally 190 or 250 mm, calibrated to 189.9 mm and 244.7 mm, respectively, by means of a Si-standard sample (NBS 640b). The Si-standard was also used to determine the exact centre of the beam on the image-plate, as well as for correction of the off-orthogonality of the plate with respect to the beam.

Images were collected on the Swiss-Norwegian Beamlines (SNBL) at ESRF, with an exposure time of 30 s. The capillary was rotated 30° during the exposure in order to increase the number of crystallites contributing to the signal. The large image-plate mode (345 mm) was employed in combination with a resolution of 100 μm. A focused beam was used for the measurements, and the size of the beam on the sample was 0.3×0.3 mm, thus covering only the central part of the 1.5 mm diameter capillary. The X-ray study was carried out in two series of experiments, with wavelengths 0.7519 Å and 0.7005 Å, respectively, and with sample–detector distances as given above.

Integration of the two-dimensional pattern was made by means of the FIT2D program [3]. The upper 2θ-limit was set to 50.0°, and the 2θ-scale was split into 5000 bins for the integration (1 step = 0.01° in 2θ). The resulting intensity patterns were subsequently transformed into a format suitable for input to the program system GSAS by Larson and Von Dreele [4], and a Rietveld refinement was performed on each complete powder pattern making use of GSAS with a profile function that includes asymmetry correction [5].

The use of a focused beam is very convenient for rapid data collection, and thus for enabling temperature scans. However, due to the inherent divergence of the beam, part of the observed peak width originates from the beam itself. There is also a capillary size effect which contributes to peak broadening. The contribution from beam divergence was determined by using a LaB_6 standard sample (intrinsic FWHM < 0.01°) in a narrow (0.3 mm) capillary. The effect of the sample size was determined by the use of a Si-sample in a 1.5 mm capillary. Before the temperature study, a diffractogram (Fig. 1) was collected at ambient temperature (RT) on one of the samples using the high-resolution powder diffractometer of Station B at SNBL, in order to optimize the starting values for the subsequent refinement of the image-plate data.

For the temperature study, a newly developed furnace [6], specially designed to be mounted on the MAR345 system, was employed. A top view of the central part of the furnace, as installed on the MAR345, is shown in Fig. 2.

The sample is heated by a set of four resistances in order to provide an approximately homogeneous temperature in the central part of the furnace. A set of five melting point standards were used in the present study to obtain an accurate calibration in the temperature range of interest. These were naphthalene ($T_m = 80.1$ °C), benzoic acid ($T_m = 122.1$ °C), *p*-anisic acid ($T_m = 183.2$ °C), all melting points with an error of ±0.2 °C. In addition the metals In (purity > 99.996%, $T_m = 156.6$ °C) and Sn (purity > 99.8%, $T_m = 231.9$ °C) were used.

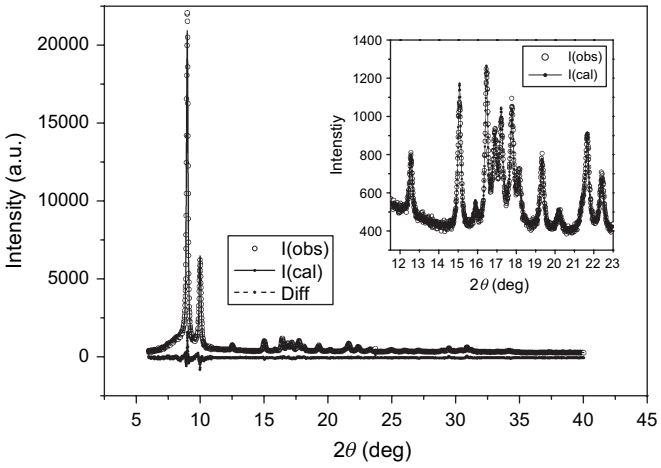

Fig. 1. High-resolution room temperature diffractogram of one of the ethylene copolymer samples (A, *cf.* Table 1). The difference pattern (Diff) between the observed and calculated data (Rietveld analysis) is shown in the lower part of the figure. The inset shows in more detail the intermediate region with several well-resolved peaks. The wavelength was 0.6479 Å.

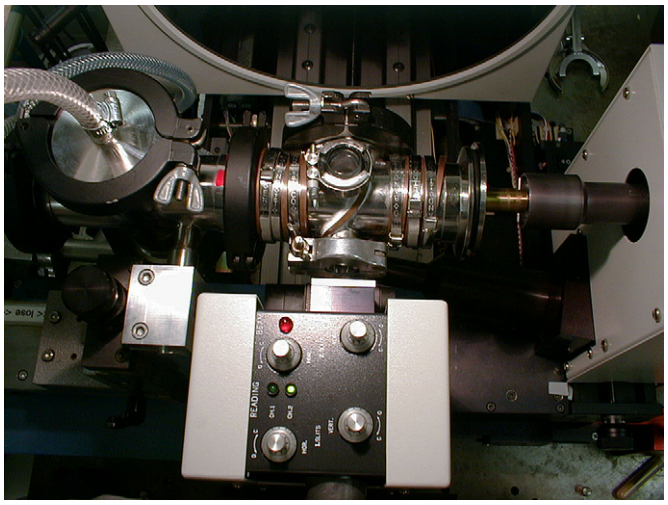

Fig. 2. Top view of the He-filled furnace used in the experiments. The sample is introduced from the right, and the beam enters at the lower side of the picture, through the MAR345 slit system.

The result of the calibration is shown in Fig. 3. During the measurements the furnace was filled with He gas providing a controlled and inert atmosphere.

The temperature cycles were executed between room temperature and a maximum of 200 °C in steps of 10–20 °C, decreasing to 5 and 2 °C, and finally to 1 °C step-sizes in the regions of most interest. Recrystallization was monitored during cooling of the melt. For samples A–C two images were collected for each temperature point with a dwell time of 150 s in between.

2.3. Differential scanning calorimetry (DSC)

A Perkin–Elmer DSC-7 instrument was used for all the DSC experiments. The instrument was calibrated with an indium standard to give the onset of melting at 156.6 °C and

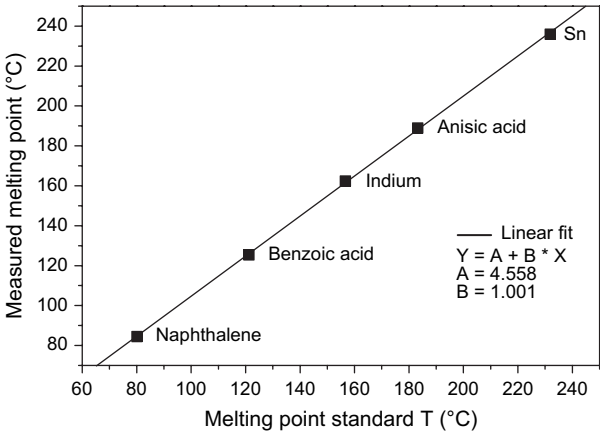

Fig. 3. Calibration curve for the furnace obtained from five different standards with melting points in the temperature range relevant for this study.

an enthalpy of fusion of 28.45 J g^{-1}. Scans were performed at a heating rate of 10 K min^{-1} in an N_2 atmosphere to avoid thermal oxidation. Approximately 5 mg of polymer was introduced into a 30 µl alumina pan with holes, which was sealed using a pan crimping tool. An empty alumina pan was used as a reference. The heating curves were corrected to the true baseline by reference to heating curves obtained with empty sample pans. Since the melting of the polymer crystals is related to the heating rate [7,8], a temperature correction function was determined [9]. For this purpose, eight polyethylene (PE) samples were chosen with different melting peak temperatures. Each sample was subjected to the same thermal history, crystallized from 200 to 25 °C at a cooling rate of 50 K min^{-1}. DSC scans were executed at different heating rates; 2, 10, 30, 60 and 100 K min^{-1}, and the peak melting temperature was identified. For each heating rate, the DSC was calibrated with respect to temperature and enthalpy of fusion, using the indium standard. Extrapolation to zero heating rate will give the true melting temperature [10–12]. The crystallinity of the polymer samples was calculated by the total enthalpy method [13,14] using the enthalpy of fusion function derived by Mathot [15].

$$\Delta_{\mathrm{fus}}H^0(T) = 293 - 0.3092 \times 10^{-5}(414.6 - T)^2 \times (414.6 - 2T)\ \mathrm{J/g}$$

where the temperature T is in Kelvin.

The DSC was also used to estimate the 1-hexene content of the polymer samples. The melting point of a polymer crystallite is related to the lamellar thickness through the Gibbs–Thompson equation [16].

$$T_{\mathrm{m}} = T_{\mathrm{m}}^0\left[1 - \frac{2\sigma_{\mathrm{e}}}{l_{\mathrm{c}}\Delta H_{\mathrm{m}}^0}\right]$$

where T_{m}^0 is the melting point of an infinite sized crystallite, σ_{e} is the lamellar fold plane interfacial energy, l_{c} is the thickness of the crystallite and ΔH_{m}^0 is the bulk melting enthalpy. The crystallite thickness is dependent on the amount of

comonomer incorporated into the polymer backbone [17]. The samples used in this study were part of a larger group, for which the 1-hexene content had been measured by the manufacturer (infrared spectroscopy) for six of the samples. From these six samples a linear calibration was made for the 1-hexene content against the peak melting temperature, when subjected to the same thermal history [9]. The 1-hexene content for the samples used in this study was thus estimated from this linear calibration.

2.4. Size exclusion chromatography (SEC)

The molecular weight (M_n) and polydispersity (M_w/M_n) of the samples were determined by means of a high temperature size exclusion chromatograph (PL-GPC210, Polymer Laboratories, UK). The setup consisted of a differential refractive index detector (Model 210RI, Viscotek, USA), a four-capillary bridge viscometer (Model 210R, Viscotek, USA), and a light scattering detector (Model PD2040, Precision Detectors, USA). The viscometer was connected in parallel with the differential refractive index detector with a flow ratio of 55:45. The light scattering detector was connected serially in front of the other two detectors. Separations were made using three PLgel 10 μm MIXED-B 300 × 7.5-mm columns, guarded by a precolumn. 1,2,4-Trichlorobenzene (TCB) was used as eluent at a flow rate of 1 ml min^{-1}. The TCB was stabilized with the antioxidant BHT at a concentration of 0.0125 wt%. The temperature used throughout the chromatography work was 160 °C. The SEC system was calibrated using polystyrene standards (Polymer Laboratories), in a narrow range of M_w/M_n with M_n ranging from 580 g mol^{-1} to 4,000,000 g mol^{-1}.

2.5. Individual sample characteristics

Five samples of different molecular weight, polydispersity and contents of 1-hexene, here labelled A, B, C, D and E, were used in these studies (Table 1).

3. Results and discussion

We observe that the samples A, D and E are very similar both in polydispersity and in cohexene content but differ in M_n. This subgroup therefore offers information on the effects of varying molecular weight. Samples A and B are similar except for the polydispersity, and samples C and D compare closely with respect to molecular weight and polydispersity, but C has a much higher content of cohexene. It is clear that the analyses of the data and the conclusions must be viewed in light of the limited number of samples.

3.1. Mass crystallinity and melting point

The crystallinity in the group of samples A, D and E having a nearly constant cohexene content decreases with increasing molecular weight. This is the expected result. It is known that the crystallinity for linear PE [18,19] as well as other homopolymers obtained from the melt [20,21] decreases with increasing molecular weight up to values of about 10^6. Except for a general reduction in crystallinity relative to the parent homopolymer [22] ethylene copolymers with a fixed comonomer content show a similar decrease in crystallinity with increasing molecular weight [23]. In agreement with the general observation of Alamo and Mandelkern [22] we also observe that sample C with the highest branching content has a lower crystallinity than sample D.

The melting temperatures were determined by two different methods, and the values obtained for a given sample in Table 1 may differ somewhat. Nevertheless, the averaged values for the samples A, D and E indicate a slight increase in T_m with increasing molecular weight. This is in agreement with the predictions for long-chain molecules [24,25]. In contrast, a decrease in melting temperature with increasing molecular weight has been reported for various ethylene/1-alkene copolymers [17,23]. This apparently anomalous behaviour was attributed to decreasing crystallite thickness in the chain direction with molecular weight. The reduced melting temperature of sample C is in agreement with many previous observations on the effect of an increasing content of branch points [23,26].

3.2. Unit cell parameters

3.2.1. Background

Following the early work by Müller on normal paraffins [27] several studies have been made of the variation of the unit cell parameters of PE with temperature, *cf.* Swan [28] and references therein. The work by Swan has been succeeded

Table 1
Characteristics of the five different ethylene/1-hexene copolymer samples used in this study

Sample	Catalyst	Reactor T [°C]	M_n[a] [g mol^{-1}]	M_w/M_n[a]	1-Hexene content[b] [mol%]	Mass cryst.[b] [%]	Melting T [°C]	
							T_m[c]	T_m[d]
A	Metallocene	97.5	16,500	2.2	0.14	74.1	136	137
B	Chromium	96	21,300	11.3	0.07	70.4	135	132
C	Metallocene	85	59,800	1.8	2.26	50.8	119	120
D	Metallocene	85	60,100	2.0	0.24	62.5	136	140
E	Metallocene	38	1,31,500	2.1	0.11	52.3	141	143

[a] Determined by SEC.
[b] Determined by DSC.
[c] Determined by DSC with an error ±0.2 °C.
[d] Determined visually.

by a number of other studies of both oriented and unoriented PE [29–39]. In most of these studies, however, only a small number of reflections was used, often only 2–6. In one case [37] 45–50 reflections were used but for a sample of uniaxially oriented PE. With one or two exceptions, radiation from a conventional X-ray source was employed, in some cases monochromatized, yielding the $K_{\alpha 1}$ emission line from the target material, in other cases only filtered, providing the $K_{\alpha 1}/K_{\alpha 2}$ doublet which will contribute to a diffraction-line broadening increasing with 2θ.

The effects of branch type and content on the unit cell parameters of ethylene copolymers have been studied by several authors. A representative summary of work up to 1989 on ethylene copolymers with different α-olefins has been presented by Howard and Crist [40]. More recent studies addressing also the impact of branch distribution have been published by Baker and Windle [26,41] and Rabiej [42].

3.2.2. Qualitative observations

Fig. 4 shows a typical image-plate pattern for one of the samples (A) collected at RT (23 °C) with 30 s exposure time. About 17 powder rings can be identified, of which the majority consists of several partially overlapping maxima. The dominating feature close to the centre of the image are the strong (110) and (200) reflections from the orthorhombic structure (*Pnam*). The outer edge of the pattern corresponds to a 2θ-value of 35°, or a *d*-value of 1.25 Å. Although not easily recognizable in this picture, the integrated intensity still shows peaks close to the edge of the detector. For the best crystalline samples a total of 27 reflections were available for Rietveld refinement.

Heating the sample will increase the atomic displacement parameters, *i.e.* an increase of B_j in the expression $\exp(-2B_j s^2)$, where $s = \sin\theta/\lambda$, which causes a general reduction of the intensity maxima. This process starts immediately upon heating, and since the effect is exponential in s^2 a reduction in peak height will be seen most clearly for reflections at large 2θ. The melting that starts later, will first break down the long-range order, thus the increase in line-width should be seen first for the high angle reflections. This is also what we observed with our samples, where the typical peak width (FWHM) of 0.3° (2θ) increased by about 20% for the peaks at highest angles prior to melting, but remained nearly constant at low angles.

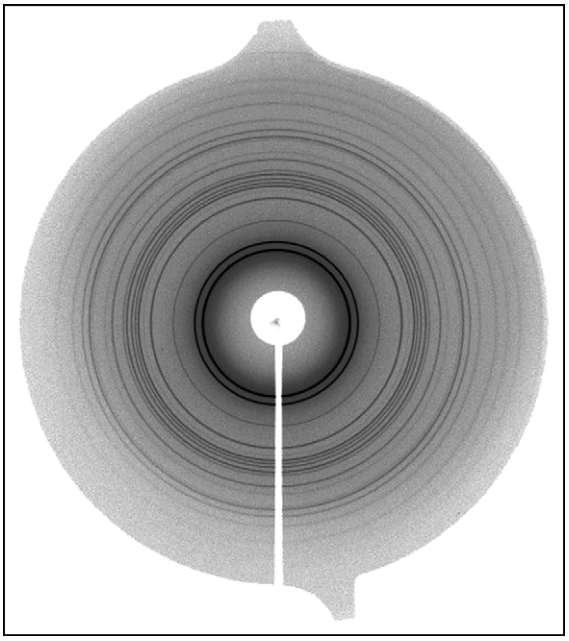

Fig. 4. 2-D pattern of one of the samples (A) at RT. The wavelength was 0.7519 Å, and the sample to detector distance was 189.9 mm.

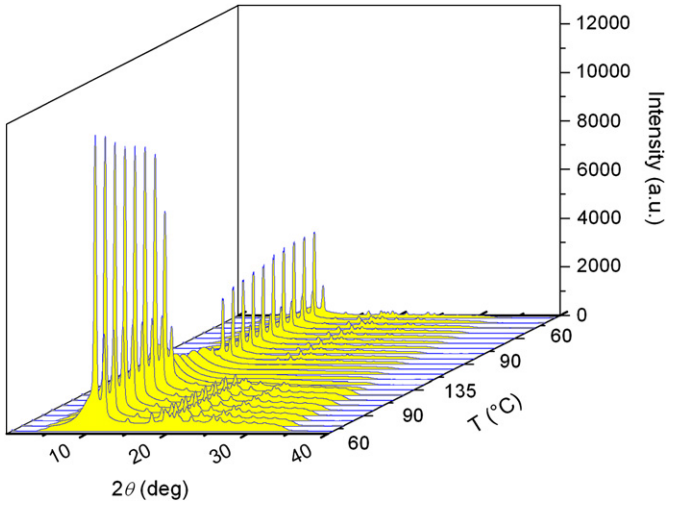

Fig. 5. 3-D pattern showing the evolution of the diffraction pattern upon heating up to 150 °C and subsequent cooling down towards RT of sample A. The leftmost group of peaks represents the heating sequence and the rightmost group represents the cooling sequence.

Fig. 5 shows the evolution of the diffraction pattern for one of the samples (A) as the temperature is raised from RT to 150 °C and then cooled back to RT. The sample recrystallizes at a temperature which was found to be approximately 5 °C below the temperature where melting starts. The peak intensities are seen to be lower in the cooling regime than in the heating regime. This is due to the compaction and redistribution of the sample in the capillary upon melting, resulting in a smaller amount of sample being hit by the 0.3 × 0.3 mm beam.

Fig. 6a shows how the dominating (110) and (200) peaks develop during recrystallization for one of the polymer samples (C) during cooling from above its T_m. In addition to the dramatic changes in peak height and shape, one also notices the displacements of the peak centres with decreasing temperature. Shifts towards higher 2θ-angles are clearly seen for the (200) maximum, reflecting the almost linear contraction of the *a*-axis with decreasing temperature in most of the *T* range below melting, *cf.* Fig. 7. Reflection (110) has contributions from both $a^* = 1/a$ and $b^* = 1/b$, mostly from the latter since $b^* > a^*$. As will be shown in more detail later, a^* increases and b^* decreases during the first stage of cooling. For sample C the reduction in b^* is nonlinear and particularly strong in the temperature range 112 → 95 °C. One would then expect that the position of the (110) peak approaches lower 2θ-values as *T* is decreased in this *T*-range, and subsequently increases slightly in 2θ at lower *T*, when the contribution from the increasing a^* starts to dominate.

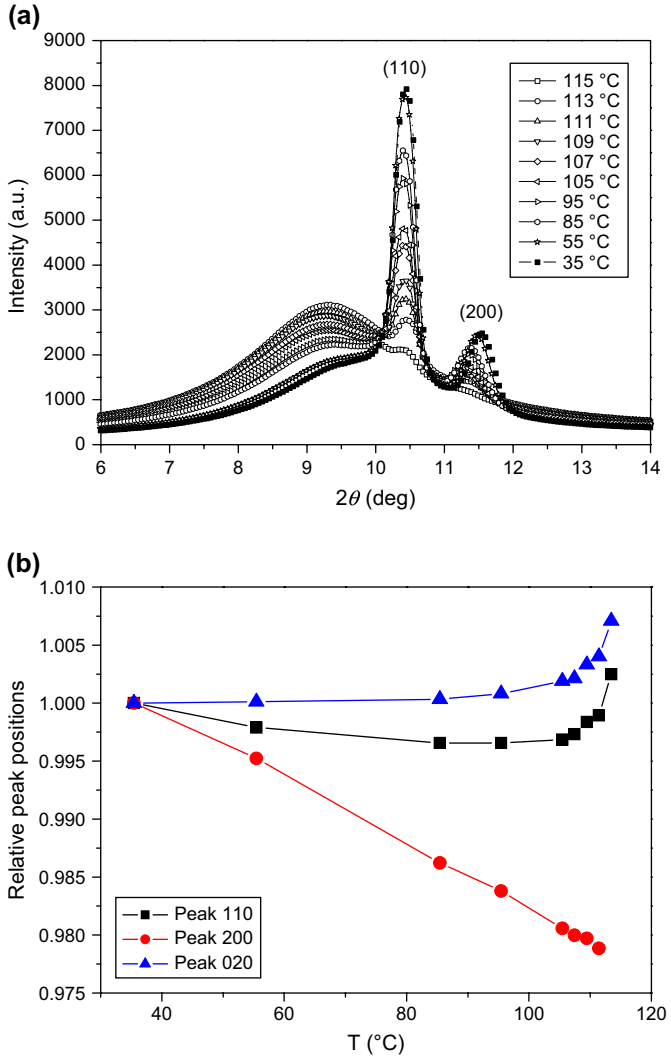

Fig. 6. (a) Evolution with temperature of the two strongest low-angle peaks of sample C as it is cooled from melting temperature to 35 °C. (b) Shifts in position with temperature of the (110), (200), and (020) peaks of sample C as it is cooled from melting temperature to 35 °C. The 2θ-values for the peak positions have been normalized to the values at the lowest temperature.

This behaviour is exactly what we observe, as demonstrated in Fig. 6b. This figure also shows the thermal shifts of the (020) peak, which is only influenced by changes in b^*: a non-linear decrease in 2θ from melting down to about 90 °C, and from there on a nearly constant magnitude of 2θ (and b^*). A more quantitative discussion of the thermal influence on the unit cell parameters based on Rietveld refinements will be given in Section 3.2.3.

The fully melted sample contains a very broad peak (amorphous contribution) centred at a d-value ~4.7 Å (2θ ~ 9.2°), which can probably be ascribed to interchain correlation [43]. There is also a smaller peak present, corresponding to a d-value of 2.19 Å, which may be the signature of an intrachain correlation.

3.2.3. Results and quantitative analyses

In the present work we have used monochromatized synchrotron radiation. In order to obtain precise values for the lattice parameters a Rietveld refinement was carried out at each temperature step for each of the samples in Table 1. Data out to 2θ = 33° comprising up to 27 reflections (hkl), some of them partly overlapping, were employed in the refinements.

Fig. 7a shows the result of Rietveld refinements at each temperature on the sample with the lowest molecular weight (A). The lattice parameters a, b, and c are shown at all temperatures, both for the heating and cooling processes. Upon heating from room temperature, there is a significant, almost linear increase in a, about 3% in the temperature range from 40 to 130 °C. After having reached the fully melted state, the sample was cooled slowly (in about 1.5 h) from 145 °C through the recrystallization stage down to 45 °C. Characteristic structures in the pattern, sufficient for applying Rietveld analysis, appear around 130 °C, but the standard deviations are relatively large in this range. The lattice constants are in general slightly smaller for a given T during cooling as compared to the heating sequence. The reduction is largest for the b- and c-axes. After recrystallization b becomes almost independent of T in the range 40 to ~100 °C. The decrease in unit cell volume is nearly linear with T during cooling. Sample A had a melting point of ~137 °C as determined visually, which is close to the value obtained from DSC measurements.

Fig. 7b–e shows the temperature effect on the lattice parameters for the other four samples, B–E, in this study. They range from intermediate to high in molecular weight, and have varying degrees of polydispersity and branching.

The sample with lowest molecular weight (A) was also the one with the highest crystallinity, a fact that is reflected in the smaller standard deviations of its lattice parameters compared to the other samples.

Interestingly, sample E showed clear signs of a cocrystallized monoclinic phase. All the other samples were purely orthorhombic (*Pnam*). The unit cell of the monoclinic phase according to Seto et al. [44] has a = 8.09 Å, b = 2.53 Å, c = 4.79 Å, β = 107.9°, *i.e.* b is the unique axis. The (001) peak of the monoclinic phase can be seen to the left of the main peak in Fig. 8, at a 2θ-value of 8.85° (d = 4.54 Å). The content of the monoclinic (*C*2/*m*) phase of this sample was estimated to 7% at room temperature. It disappeared gradually with increasing temperature, and was no longer present at T = 120 °C. After annealing there were no traces of this phase. Sample E was prepared at a low reactor temperature (see Table 1), and it is possible that a partial transformation to the monoclinic phase was induced by shear–stress deformation during the preparation [45].

The values for the lattice parameters at $T \approx 55$ °C, as extracted by Rietveld refinements, are shown in Table 2 for all samples. Values are given both before melting and after recrystallization.

The unit cell parameters of ethylene copolymers depend, as for the parent homopolymers, on the crystallization and annealing conditions due to the impact of these factors on the thickness of the crystalline lamellae. A roughly reciprocal relationship between the base area ab, and the average lamellar thickness has been reported [40,46–48]. The influence of

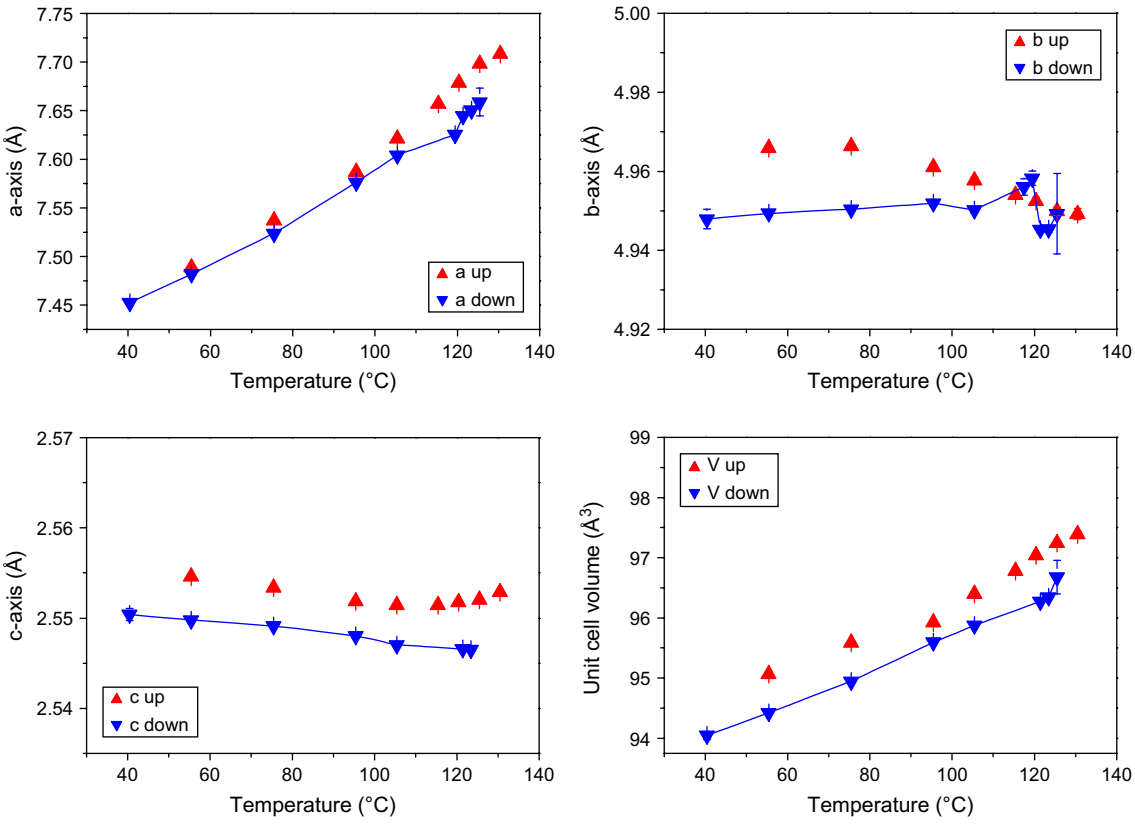
a-axis (Å)
Temperature (°C)
a up
a down
b-axis (Å)
b up
b down
c-axis (Å)
c up
c down
Unit cell volume (Å3)
V up
V down

(a)

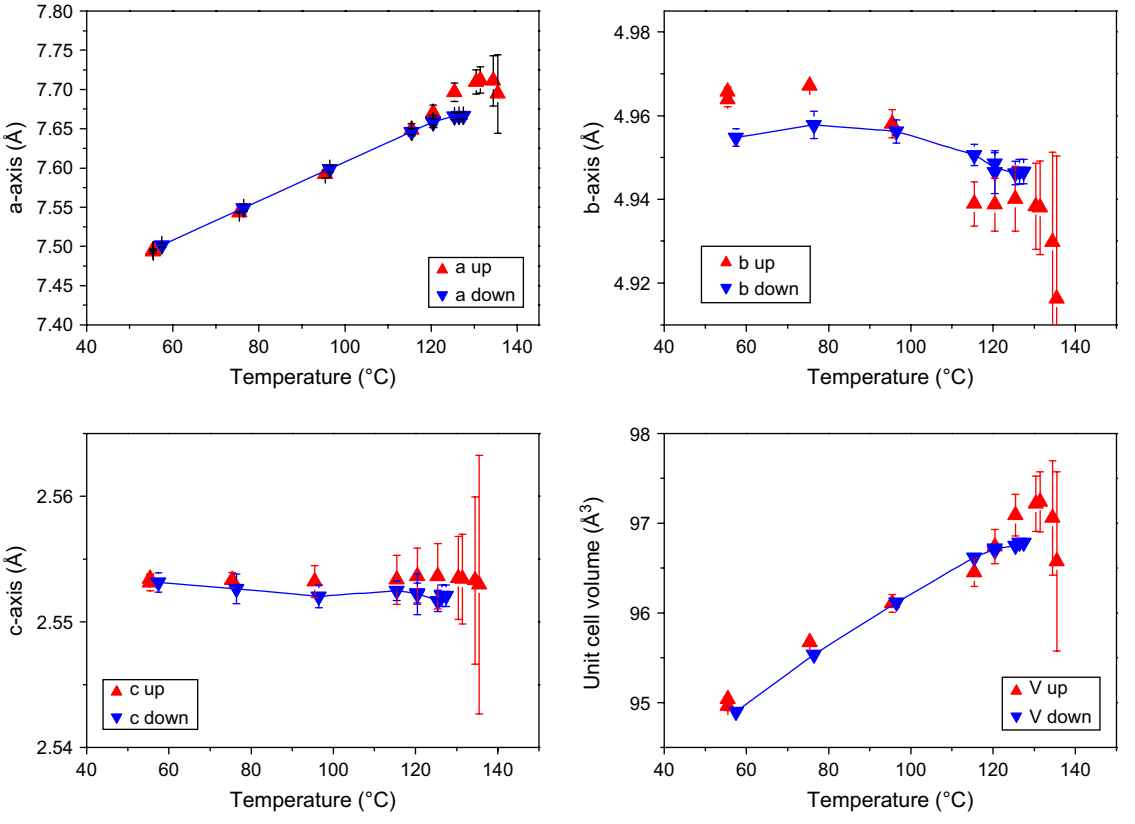
a-axis (Å)
Temperature (°C)
a up
a down
b-axis (Å)
b up
b down
c-axis (Å)
c up
c down
Unit cell volume (Å3)
V up
V down

(b)

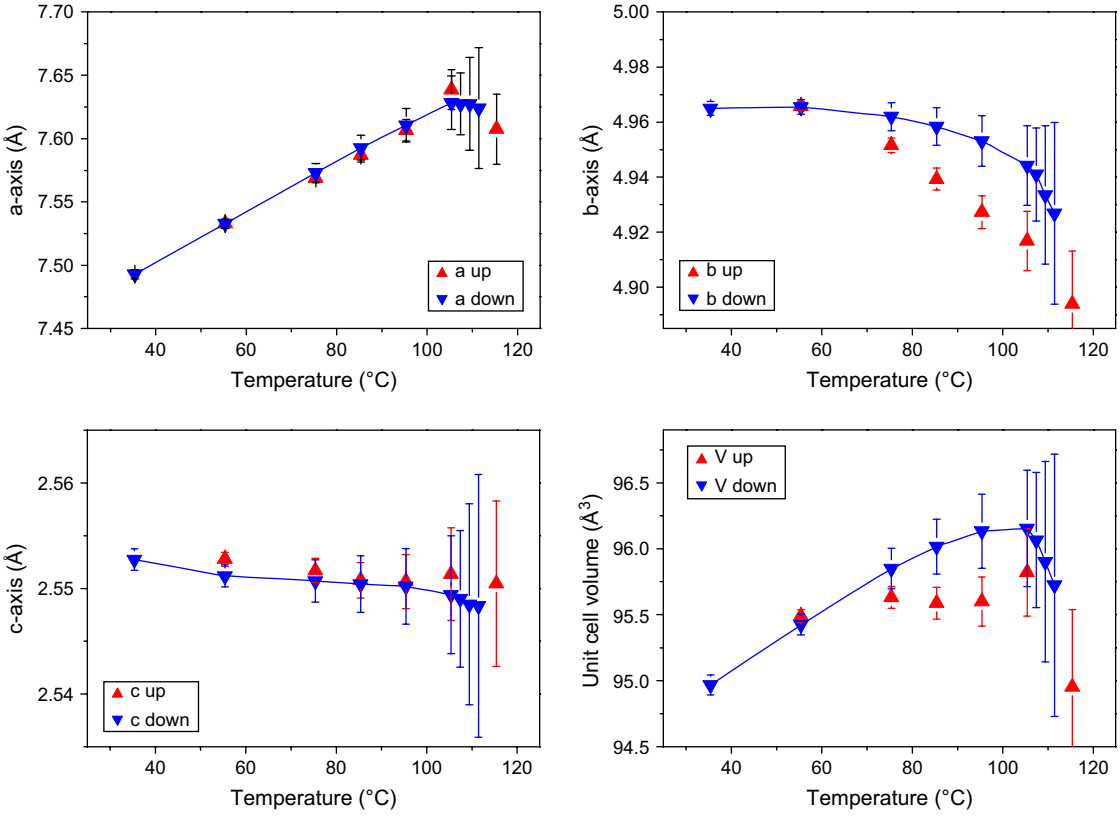
a-axis (Å)
Temperature (°C)
a up
a down
b-axis (Å)
b up
b down
c-axis (Å)
c up
c down
Unit cell volume (Å^3)
V up
V down

(c)

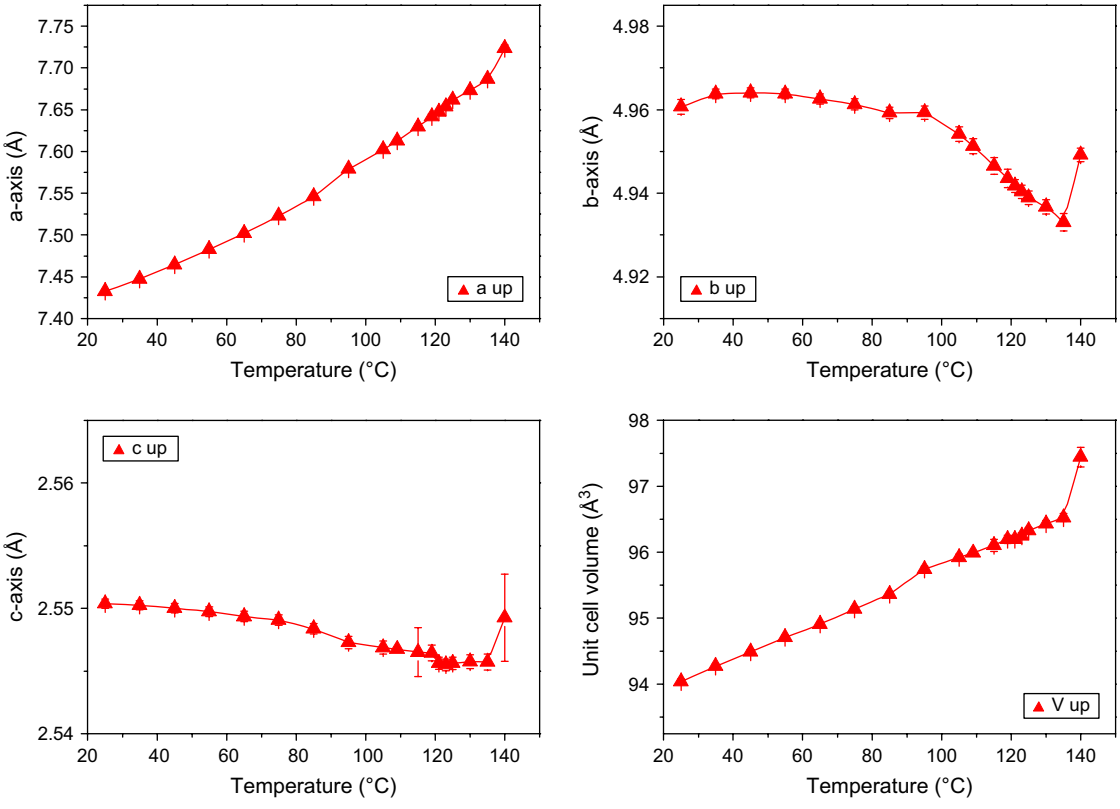
a-axis (Å)
Temperature (°C)
a up
b-axis (Å)
b up
c-axis (Å)
c up
Unit cell volume (Å^3)
V up

(d)

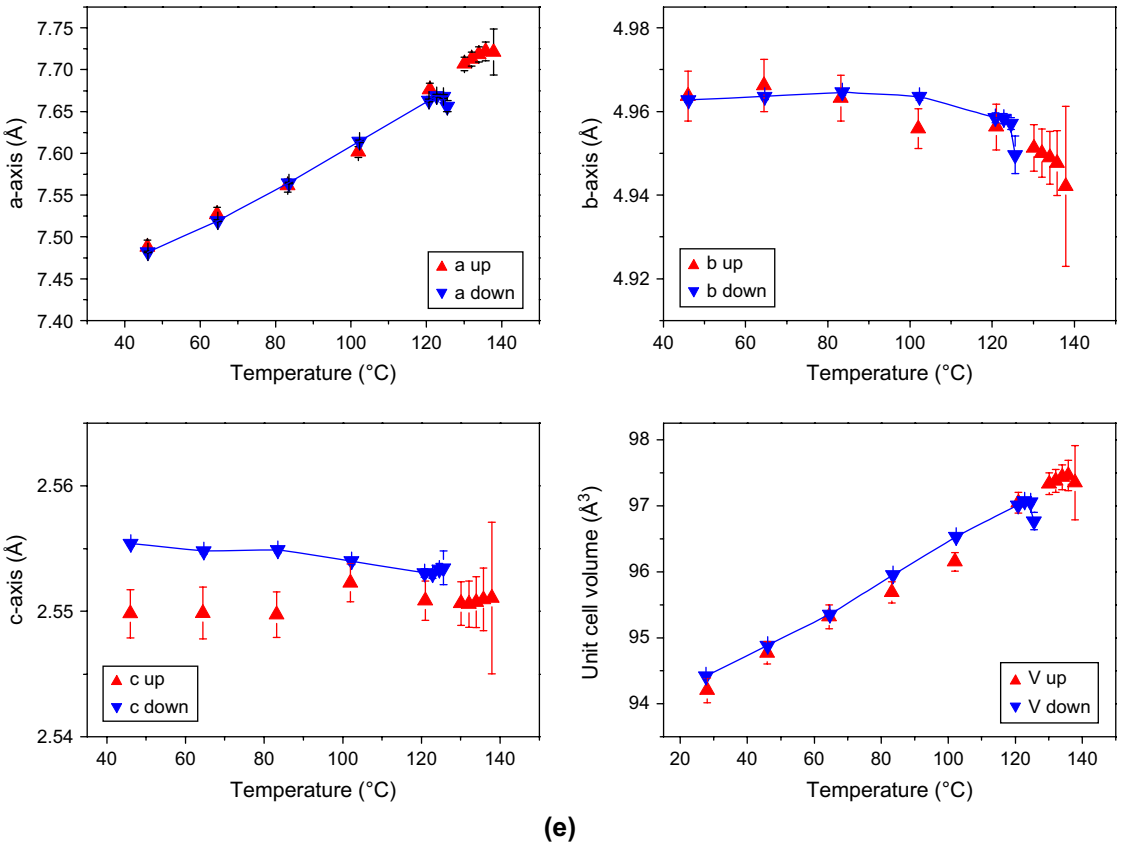

Fig. 7. (a)–(e) Evolution with temperature of lattice parameters and unit cell volume of samples A–E (Table 1) based on Rietveld refinement at each temperature. As a guide to the eye, a line has been drawn through the points for the lattice constants corresponding to the cooling regime. For sample D only the heating sequence is shown, since the data for the cooling sequence was found to be corrupted.

concentration, size and regularity of the side-chain branches is also well documented, *cf.* Howard and Crist [40], Baker and Windle [26] and references therein. For unoriented ethylene copolymers it is generally found that the *a*- and *b*-axes, normal to the chain direction, are longer than in the parent homopolymers. Methyl, and to a lesser extent ethyl branches, induce expansion primarily of *a* but also *b*, proportional to the branch content up to a certain level, after which these parameters remain constant. For longer branches like propyl and butyl, there appears to be no further expansion, independent of branch content [40]. This result, which is challenged [26], has been interpreted to indicate that the shortest branches, in particular methyl, are incorporated in the crystalline lamellae, but with increasing content further accommodation in the crystalline environment becomes progressively rare. The longer branches appear to be excluded from the lamellae, thereby inducing strain and a concomitant reduction of lamellar thickness. It is reasonable to assume, however, that there is no distinct limit in branch size leading to a uniform exclusion of the branching unit. In fact, ^{13}C NMR measurements have indicated that *n*-butyl, *n*-hexyl up to *n*-decyl branches can be incorporated in the crystal by fractions of about 6% [49]. In summary, the average volume of a copolymer unit cell can increase as a result of two different deformation mechanisms: a progressive inclusion of short side-chain branches in the crystalline lamellae, and a reduction of crystal thickness caused by exclusion of longer side chains which will induce surface stress on the lamellae [42].

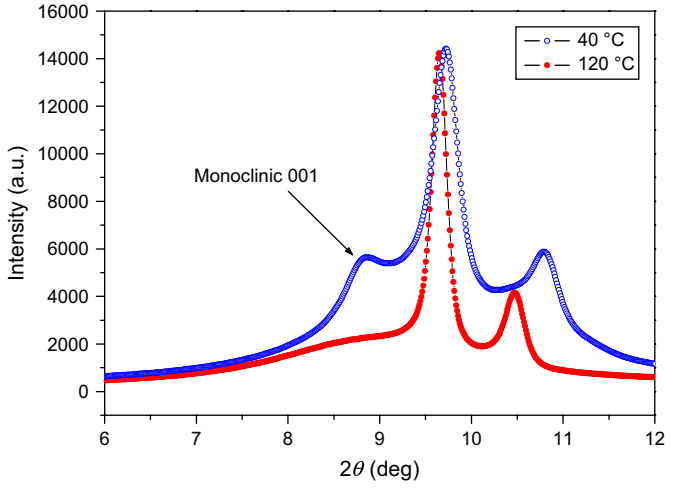

Fig. 8. Low-angle part of the diffraction pattern for sample E, showing one peak corresponding to the monoclinic phase ($T = 40$ °C).

The 1-hexene comonomer will generate a polymer with *n*-butyl branches presumably to a large extent being excluded from the crystalline lamellae. The *a*-axis is the one most

Table 2
Lattice parameters a, b, and c calculated at $T \approx 55$ °C for the five samples studied

Sample	a (Å) before/after	b (Å) before/after	c (Å) before/after
A	7.4888 (7)/7.4821 (7)	4.9659 (5)/4.9494 (5)	2.5546 (2)/2.5498 (1)
B	7.4953 (16)/7.5016 (29)	4.9657 (12)/4.9548 (21)	2.5534 (4)/2.5531 (8)
C	7.5328 (22)/7.5329 (37)	4.9658 (16)/4.9655 (26)	2.5528 (7)/2.5512 (10)
D	7.4830 (17)	4.9638 (12)	2.5497 (4)
E	7.4881 (82)/7.4820 (9)	4.9637 (60)/4.9628 (7)	2.5498 (19)/2.5554 (2)

The two values (before/after) listed for each lattice parameter refer to the values before melting and after recrystallization, respectively. For sample D only the values before melting can be given. The time spent for passing through annealing (defined here as the time between $T_{recryst}$ +5 °C and $T_{recryst}$ −10 °C) was approximately 35 min.

strongly influenced by different sample characteristics, *cf.* Table 1. Samples A, D and E which are very similar both with respect to cohexene content and polydispersity, but are different in molecular weight and crystallinity, have very similar lengths of the *a*-axis up to melting. Annealing brings about a small shortening of *a* which becomes identical for samples A and E (sample D has been excluded from this comparison due to impaired diffraction data from the cooling sequence). Sample B has a slightly longer *a* than samples A, D and E, and it increases significantly after annealing. This sample has the largest polydispersity which is the main difference from sample A. The influence of a larger content of *n*-butyl branches is clearly seen for sample C which has the largest *a*, and this parameter remains unchanged after annealing.

We have calculated the coefficient of thermal expansion (CTE) in the three axial directions for the five samples and have used the development during cooling from recrystallization to 45 °C (55 °C for sample B) along *a*, and in the *T*-range $T_m - 30$–45 °C along *b* and *c*. For sample D values from the heating sequence were used for this calculation. The results are shown in Table 3.

There is a nearly linear decrease in *a* with temperature after annealing, the parent α_a are in the range $(26–34) \times 10^{-5}$ K^{-1}, with the larger values for the most crystalline samples. All samples except C show a slightly nonlinear increase in the expansion of *a* as *T* approaches T_m, the behaviour during cooling is more linear, see Fig. 7. Below this premelting range in *T*, the effect of temperature on *a* seems to be reversible; there is practically no difference between the heating and cooling sequences. Values for α_a obtained for various unoriented and oriented samples of PE and HDPE reported up to 1999 have been compiled by Tashiro et al. [37]. Most of the authors referred there have not given data above room temperature. Swan [28] reported an α_a of 22×10^{-5} K^{-1} at 303 K, increasing to 57.8×10^{-5} K^{-1} at 411 K, close to melting, for an unoriented HDPE.

Table 3
Linear expansion coefficients ($\times 10^{-5}$ K^{-1}) with esd's for samples A–E

Sample	$\alpha_a \times 10^{-5}$ K^{-1}	$\alpha_b \times 10^{-5}$ K^{-1}	$\alpha_c \times 10^{-5}$ K^{-1}
A	32 ± 1	1 ± 1	-2.0 ± 0.2
B	32 ± 1	-2 ± 1	-0.6 ± 0.2
C	26 ± 1	-2 ± 1	-1.9 ± 0.4
D	34 ± 1	-2 ± 1	-1.9 ± 0.3
E	29 ± 1	1 ± 1	-8.0 ± 0.1

Values have been calculated for the cooling sequence, *i.e.* after recrystallization, in the temperature range from recrystallization to 45 °C along *a*, and from $T_m - 30$ °C to 45 °C along *b* and *c*. Values from the heating sequence were used for sample D.

The length of the *c*-axis, along the C–C zig-zag chain, before melting is closely similar for samples A–C, *c* is slightly shorter for samples D and E. After annealing there are small but significant changes in opposite directions in this parameter for samples A and E, a contraction in the former and an expansion in the latter. The overall effect is an apparent small increase in *c* with molecular weight. A small negative dependence on *c* with ethyl branch content has been reported previously [40]. A similar trend with butyl branching cannot be ascertained from the present study. The averaged *c*-value before melting equals 2.5521 Å, and is unchanged (2.5524 Å) after recrystallization.

A common feature for all samples is a negative linear expansion along *c*, α_c is in the range -0.6 to -2.0×10^{-5} K^{-1} for samples A–D, and somewhat more negative for sample E, -8.0×10^{-5} K^{-1}. A small contraction along the PE chain axis with increasing *T* was first reported by Kobayashi and Keller [29] and has been confirmed in many studies since then. According to Chen et al. [50] the negative expansion along the polymer chain is a general feature for most if not all polymers, with α_c in the range -1 to -5×10^{-5} K^{-1}. The theory of chain contraction with increasing temperature in polymer crystals has been developed by several workers, providing good agreement between calculations and experiment [50,51]. Transverse torsional and bending modes of vibration in the C–C–C sequence of the polymer chain are excited at temperatures 100–300 K, *cf.* Vettegren et al. [52] and references therein. With increasing amplitudes of vibration the projection of the molecular skeleton onto the molecular axis will become progressively shorter resulting in a longitudinal contraction.

At $T \approx 55$ °C, before melting, *b* is identical for all five samples, the average value is 4.9650 Å. No effect from an increased content of cohexene is apparent. After annealing there is a distinct contraction in *b* for the most crystalline samples A and B, indicating a denser packing in this direction. A similar contraction does not apply to the least crystalline samples C and E.

The thermal response of the *b*-axis is remarkable. In the lower range of *T* both during heating and cooling, *b* remains constant, $\alpha_b = 0$ within 2σ from RT to about $T_m - 40$ °C.

Above the latter temperature and up to melting α_b becomes increasingly negative. This nonlinear change in b, which is particularly prominent during heating, is contrary to the observations of Hsie and Hu [53] and Tashiro et al. [37]. However, these studies were made on ultra-high molecular weight fibres and uniaxially oriented HDPE (stretching of a melt-quenched sample), respectively, and are not directly comparable to our results. Swan [28] on the other hand, in his study of a linear unoriented HDPE observed a relatively constant b above room temperature, and then, with increasing T, a change to contraction, with $\alpha_b = -7.2 \times 10^{-5}\,K^{-1}$ at 411 K. A very similar thermal behaviour of b close to melting was reported by Pereira et al. [36], in this case the sample was a hot-drawn HDPE. The observation was not further discussed by the authors.

Since all samples in the present study, to less extent sample A, exhibit a pronounced nonlinear contraction of b prior to melting, we believe that this is a real effect related to changes in the structure taking place above a certain threshold temperature.

3.3. Structure parameters

3.3.1. Structure refinements

In order to study the structural response to changes in T we have carried out least-squares refinements for all samples at RT, at 15–20 °C below T_m during heating, and T at the end of the cooling sequence. For sample C we have followed the evolution of structure in more detail by refinements at several temperatures both during heating up to $T = 115$ °C and after recrystallization and cooling from $T \approx 111$ °C down to $T = 35$ °C.

Even for the best crystalline polymer samples the diffraction data is of modest quality, and is further reduced, also in quantity, by decreasing crystallinity and increasing temperature. A major purpose of the refinements was to obtain parameters describing the packing and the rotational orientation of the chains. In the course of this work we obtained as well evidence for a pronounced asymmetry in the C–C–H angles which is also important for the interchain contact distances.

Characteristic structure parameters of the aliphatic hydrocarbon chain itself are well established from several X-ray diffraction studies of single crystals of *n*-alkanes and various lipid components such as long-chain fatty acids and alcohols, glycerides, etc. Therefore, to minimize the impact of differences in quality and quantity between the various data sets on the results it was decided to impose two constraints on the refinements: bond lengths of C–C = 1.52 Å, and C–H = 1.00 Å. A C–C bond length of 1.52 Å is a typical value obtained from RT refinements of *n*-hydrocarbon chains, see *e.g.* the diffraction studies of two forms of stearic acid [54,55]. This mean value contains a slight apparent shortening (which implies also a slight enlargement of the C–C–C angle) due to relatively large thermal oscillatory vibrations of the chain at RT, and as well to the effect of bonding density not being taken properly into account by the usual spherical model for the C atom. The C–H bonding distance of 1.00 Å reflects a well documented apparent shortening by about 0.10–0.12 Å in standard X-ray diffraction studies. The shortening is caused by the pronounced asphericity of the electron density distribution about the nucleus of the bonded H atom. After completion of each refinement, the C–H bonding distances were expanded to 1.10 Å, which is a mean value corrected for thermal effects obtained for C(sp^3)–H bonds from precise neutron diffraction studies [56–58]. This value was used for the calculation of contact distances and angles.

3.3.2. Results

A perspective view of the orthorhombic structure of PE illustrating the stacking of adjacent polymer chains is shown in Fig. 9. The structure is completely defined by the unit cell parameters and the positional and displacement parameters for one C and two H atoms.

There are three types of interchain H···H contacts: H1···H2 (type I) approximately along $a \pm 0.6b$, H2···H2 (type II) approximately along $(b \pm c)$, and H1···H1 (type III) in which each H1 forms identical contacts to four H1 in two adjacent chains translated ½$(a \pm b)$. Of these only type I is a short H···H contact. The interchain contacts are directly related to two structural features: an asymmetry in the C–C–H valency angles and the setting angle ϕ, defined as the angle between the C–C zig-zag chain running through the origin and the *bc*-plane[1]. The contact distances, the C–C–H angles, and the setting angles have been calculated from the refined coordinates for all five samples at various temperatures. We found that the type III contact distances are remarkably constant, being in the range 2.92–2.97 Å for all the samples of this study, including four additional samples that were not subjected to thermal cycling. This range also holds at elevated temperatures. Therefore, we have included in the present survey only the calculated type I and type II contacts. For clarity only the two types of contact are marked in Fig. 9.

The results for all the samples are given in Table 4.

We have followed the development of these parameters in more detail for one of the samples (C) both during heating and cooling. The results are shown in Table 5.

3.3.3. The impact of temperature, melting and recrystallization on the structure

Before discussing the results we note that the calculated H···H contact distances for sample D at 45 °C after cooling are less reliable due to impaired data. The cocrystallized monoclinic phase in sample E (*cf.* Fig. 8) prohibits a meaningful refinement of these contacts at low T below melting, and the calculated values have been omitted from Table 4. A conspicuous structural feature, common to all samples, is a strong asymmetry in the C–C–H valency angles, the average values for C–C–H1 and C–C–H2 (in both cases excluding sample E) are 115.4° (114.6–116.1°) and 97.8° (95.4–99.6°), respectively, with ranges in parentheses. This asymmetry is a unique feature, apparently a means to accommodate inherent strain in

[1] Two different definitions of the setting angle can be found in the literature. We follow the original definition by Bunn [59], *cf.* also [60].

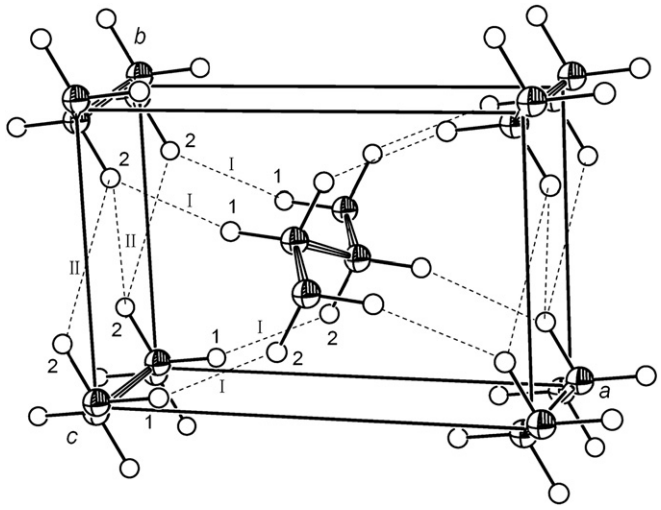

Fig. 9. Perspective view of the orthorhombic chain packing of PE. The interchain H···H contacts I and II are shown as dotted lines. Hydrogen atom H1 and H2 are labelled 1 and 2, respectively.

the polymer structure. The lateral packing of the hydrocarbon chains in PE can be described by an orthorhombic subcell of type O⊥ [61] which is a very common type of packing adopted by many long-chain compounds. A low-temperature X-ray diffraction study of the structure of 1,2-*sn*-dipalmitoylglycerol which has two chains in the orthorhombic O⊥ packing gave no indication of an angular asymmetry. The refinement which included the H atoms yielded 96 C–C–H angles associated with the 12C atoms of the central part of the chains in the range 106–112°, with a mean value of 109.0° [62].

Table 4
H···H contact distances of types I and II, C–C–H valency angles and setting angles ϕ calculated at RT, at 15–20 °C below T_m during heating, and T at the end of the cooling sequence for samples A–E

	A	B	C	D	E
I (Å)	2.27	2.32	2.33	2.23	–
	2.26	2.38	2.25	2.25	2.35
	2.34	2.40	2.30	2.42	2.33
II (Å)	2.82	2.73	2.75	2.87	–
	3.06	2.80	2.99	3.13	3.05
	2.71	2.70	2.81	2.63	2.77
C–C–H1 (°)	115.0	114.6	116.0	116.1	–
	119.4	118.2	118.4	119.0	115.7
	116.1	116.9	116.7	114.0	116.4
C–C–H2 (°)	96.8	99.6	99.2	95.4	–
	90.6	96.6	91.6	88.2	89.2
	100.0	100.1	97.5	102.5	98.2
ϕ (°)	48.4 (2)	47.4 (1)	48.1 (1)	49.3 (1)	48.4 (2)
	51.6 (2)	50.5 (2)	50.4 (3)	53.5 (3)	54.4 (3)
	48.0 (1)	50.2 (5)	48.4 (2)	47.7 (2)	49.5 (2)
T (°C)	RT	RT	RT	RT	RT
	120	120	105	121	121
	40	57	35	45	45

The esd's are in the ranges 0.01–0.03 Å for the contacts, 0.3–0.9° for the C–C–H angles and 0.1–0.5° for the setting angles. For each parameter the temperatures of the measurements yielding the values in the three lines is given at the bottom of the table.

Heating sequence prior to melting: significant changes in structure occur with increasing T. The asymmetry in the C–C–H angles becomes larger, at 15–20 °C below T_m the average values for C–C–H1 and C–C–H2 are 118.1° and 91.2°, respectively, the most noteworthy change being an average decrease of about 6.5° in the C–C–H2 angles. The H2 atoms are involved in both contacts I and II. Secondly, there is a general increase in the setting angles, the average change from RT to 15–20 °C below T_m is about +3.8°. An increasing setting angle implies a clockwise rotation of the chains running through the corners of the cell, and a corresponding anticlockwise rotation of the central chain. The consequences of these changes are relatively minor for the type I contacts, both positive and negative shifts occur. The type II contacts expand significantly with increasing T, at 15–20 °C below T_m the average lengthening is 0.2 Å. The data for sample C (Table 5) show that the largest changes take place from RT up to about 85 °C and further indicate that close to melting both the type II contacts and ϕ begin to decrease, *i.e.* a reversal of the previous development.

Cooling sequence following melting and recrystallization: there are only small shifts in the type I contacts at the end of the cooling sequence for the five samples (Table 4); the results indicate a general increase relative to the values at RT before heating. The distances after recrystallization and cooling are in the range 2.30–2.40 Å. The type II contacts are shortened compared to their values 15–20 °C below T_m. Data for sample C suggest that this contraction is caused by the melting and recrystallization process, and that the distances do not change much during the subsequent cooling. Excluding the less reliable value for sample D, the final type II contacts are in the range 2.70–2.80 Å, with the shorter ones for the most crystalline samples. The asymmetry in the C–C–H angles decreases in a manner parallel to the development of the type II contacts. The average values at the lowest T after the cooling sequence are 116.0° (C–C–H1) and 99.7° (C–C–H2). For the most crystalline samples A, B and D, the final average C–C–H2 angle is 100.9°. The setting angles decrease with decreasing T, the average change relative to the values at 15–20 °C below T_m is −3.3°.

An increase of the setting angle ϕ with T has been observed by others. Iohara et al. [63] reported changes with T in the x and y coordinates of the C atom implying a small rotation of the chain planes towards the *ac*-plane, *i.e.* an increase of ϕ with increasing T (note alternative definition of setting angle in [63]). Tashiro et al. [37] have confirmed this observation from more accurate data, and reported a nearly constant ϕ of HDPE below 283 K, from there on increasing with increasing T. They also observed that the setting angle of HDPE is larger than that of an ultra-drawn PE sample in the whole temperature region 173–363 K. However, these authors did not observe that the chain rotation is reversible.

The asymmetry in the C–C–H angles, and its development during heating and the subsequent cooling sequence is consistent for the five samples. However, the angles deviate substantially from the normal range of values and correspond to an increased energy. The use of constraints for the bond lengths

Table 5
H···H contact distances of types I and II, C–C–H valency angles and setting angles ϕ calculated for sample C at various temperatures both during heating and cooling

Heating T (°C)	RT	55	75	85	95	105	115
I (Å)	2.33	2.28	2.26	2.25	2.25	2.25	2.23
II (Å)	2.75	2.86	2.92	2.95	2.95	2.99	2.93
C–C–H1 (°)	116.0	117.3	117.9	118.2	118.5	118.4	118.7
C–C–H2 (°)	99.2	96.0	94.2	93.1	92.6	91.6	92.8
ϕ (°)	48.1	48.8	49.6	50.0	50.1	50.4	49.6
Cooling T (°C)	111	105	95	85	75	55	35
I (Å)	2.33	2.34	2.33	2.32	2.32	2.32	2.30
II (Å)	2.82	2.84	2.85	2.85	2.84	2.82	2.81
C–C–H1 (°)	117.2	117.6	117.5	117.4	117.2	116.8	116.7
C–C–H2 (°)	96.2	95.8	95.6	95.8	96.2	97.1	97.5
ϕ (°)	49.0	50.0	50.0	49.9	49.6	49.1	48.4

The esd's are in the ranges 0.01–0.05 Å for the contacts, 0.4–0.7° for the C–C–H angles and 0.2–0.4° for the setting angles.

in the refinements could possibly affect the magnitude of the calculated angle values. In order to check this possibility we have carried out unconstrained refinements of one of the samples (C) at different temperatures. The C–C–H angles were very little altered, the largest shift being 2 esd. Even if there is still some doubt about the magnitudes of these angles and of the changes in them, we believe that the observed effect is real.

3.3.4. A model for enhancing crystalline order

A common behaviour of all the samples is an increase of the type II contacts by ~0.2 Å on heating from RT up to about 15–20 °C below T_m, and a concomitant increase of the C–C–H angular asymmetry by ~10° and of the setting angle ϕ by ~+3.8°. Melting and recrystallization apparently bring about a shortening of these contacts, and they do not change much in length during the subsequent cooling. Both the angular asymmetry and the rotation of the chain planes are reversed with decreasing T and the absolute changes are of about the same magnitude as those taking place during heating. The contracted C–C–H2 angles become slightly larger, *i.e.* attain more normal values than before the heating sequence.

The type II H···H contacts are diagonal in the *bc* plane. We have found that the *b*-axis remains constant both during heating and cooling in the range from RT to about $T_m - 40$ °C. Above this temperature and up to T_m there is a nonlinear and increasing contraction of *b*, which is particularly prominent during heating. The *c*-axis shows a small linear contraction with increasing T. Thus the observed changes in the interchain type II contact distances cannot be explained by the thermal behaviour of the *b*- and *c*-axes. Instead, they must be attributed to atomic and molecular movements which occur in a T dependent reversible manner.

Polyethylene and other polymers form superstructures when grown from the melt, most common among which are spherulites, spherical symmetrical aggregates with length scale 0.5–200 μm, arising mainly as a result of the radial growth of individual chain-folded lamellae from common branch points [64–66]. The generally accepted picture of a spherulite is a body consisting of diverging and twisting stacks of lamellae with amorphous interlayers, the layer planes being parallel to the speherulite radius, which also coincides with the direction of the *b*-axis [67]. Melting and recrystallization is a cleansing process creating an increased order of the material, *i.e.* in the crystallinity. It is tempting to speculate that the thermally induced 'breathing' motion of the polymer, which involves atomic displacements as well as rotation of the chain planes leading in turn to a lengthening of the interchain distance in the *bc* plane, is a prerequisite for an enhancement of crystalline order, mainly in the *b* direction, in a process which for our samples involves exclusion of butyl branches from the lamellae and presumably also a deport of amorphous material radially outwards in the spherulites. The shortening of the type II contacts and the reversal of angular asymmetry and chain rotation which follows immediately upon melting and recrystallization seems to support such a mechanism, and the detailed sequence of events suggests that this process starts prior to melting.

4. Conclusions

The use of a highly intense and well-collimated X-ray beam from a third-generation synchrotron source, combined with an area detector with online readout capabilities, allows high quality powder patterns of polyethylene to be obtained with exposure times of less than 1 min.

We have characterized five polyethylene samples of different molecular weight, polydispersity and contents of 1-hexene using a focused, monochromatic, synchrotron beam together with an area detector to record the powder diffraction pattern. A total of more than 60 measurements were carried out in the temperature range 23–200 °C, and a full Rietveld refinement was made on each data set in the temperature range accessible for this kind of analysis. The exposure time per image was typically only 30 s.

The linear coefficients of thermal expansion (CTE) for the orthorhombic lattice parameters were found to be dependent on molecular weight, crystallinity and cohexene content. The CTE was found to be always positive along the *a*-axis with the larger values for the most crystalline samples, and slightly negative along *c*. These results are in agreement with many previous studies of polymer chains. The thermal response along *b* is more complex, in most cases differing

significantly in the heating and cooling sequences. The parent CTE, α_b, was found to be zero within 2σ for all samples in the temperature range from RT to about $T_m - 40\,^{\circ}C$ when it becomes increasingly negative until melting takes place. The unit cells expand nearly linearly in the temperature range from RT to about 20 °C below T_m.

A common development in all the samples is an expansion by ~0.2 Å of the interchain H···H contacts in the *bc*-plane on heating from RT up to about 15–20 °C below T_m. This expansion can be related to an increase of the C–C–H angular asymmetry by ~10° and of the setting angle ϕ by ~+3.8°. Melting and recrystallization bring about a shortening of these contacts, and they do not change much in length during the subsequent cooling. Both the angular asymmetry and the rotation of the chain planes are reversed with decreasing T and are of about the same magnitude as the increase during heating.

The detailed sequence of thermally induced structural changes suggests that increase of crystalline order takes place predominantly in the *b* direction, in a process which may involve amorphous material to be expelled radially outwards in the spherulites, and for our samples a rejection of butyl branches from the lamellae.

Acknowledgements

Assistance from the staff at the Swiss-Norwegian Beamlines at ESRF is gratefully acknowledged. K.D.K. acknowledges financial support from the Research Council of Norway (project number 100822/431). P.V.H. acknowledges the financial support from the Research Council of Norway under the Reactor Technology in the Petrochemistry and Polymer Industry (REPP) Programme.

References

[1] Rietveld HM. J Appl Crystallogr 1969;2:65–71.
[2] Young RA. In: Young RA, editor. The Rietveld method, (International union of crystallography monographs on crystallography). Oxford University Press; 1993. p. 1–38.
[3] Hammersley A. FIT2D v. 10.31. Grenoble, France: ESRF; 1999.
[4] Larson AC, Von Dreele RB. Los Alamos Natl. Lab. Rep. 1987. LA-UR-86-784.
[5] Finger LW, Cox DE, Jephcoat AP. J Appl Crystallogr 1994;27:892–900.
[6] Estermann M, Reifler H, Steurer W, Filser F, Kocher P, Gauckler LJ. J Appl Crystallogr 1999;32:833–6.
[7] Wunderlich B. Macromolecular physics, vol. 3. New York: Academic Press; 1980.
[8] Gedde UW, Jansson J-F. Polymer 1983;24:1521–31.
[9] Hemmingsen PV. Phase equilibria in polyethylene systems, PhD Thesis. Norwegian University of Science and Technology, Trondheim, 2000.
[10] Yadav YS, Jain PC, Nanda VS. Thermochim Acta 1985;84:141–50.
[11] Höhne GWH. In: Mathot VBF, editor. Calorimetry and thermal analysis of polymers. Munich: Hanser Publisher; 1994 [chapter 3].
[12] Richardson MJ. In: Mathot VBF, editor. Calorimetry and thermal analysis of polymers. Munich: Hanser Publisher; 1994 [chapter 4].
[13] Gray AP. Thermochim Acta 1970;1:563–79.
[14] Blundell DJ, Beckett DR, Willcocks PH. Polymer 1981;22:704–7.
[15] Mathot VBF. Polymer 1984;25:579–99.
[16] Gedde UW. Polymer physics. London: Chapman & Hall; 1995.
[17] Alamo RG, Chan EKM, Mandelkern L, Voigt-Martin IG. Macromolecules 1992;25:6381–94.
[18] Mandelkern L, Allou AL, Gopalan M. J Phys Chem 1968;72:309–18.
[19] Mandelkern L. J Phys Chem 1971;75:3909–20.
[20] Alamo R, Fatou JG, Guzmán J. Polymer 1982;23:374–8.
[21] Magill JH. Makromol Chem 1986;187:455–62.
[22] Alamo RG, Mandelkern L. Macromolecules 1991;24:6480–93.
[23] Alamo RG, Mandelkern L. Macromolecules 1989;22:1273–7.
[24] Flory PJ, Vrij A. J Am Chem Soc 1963;85:3548–53.
[25] Fatou JG, Mandelkern L. J Phys Chem 1965;69:417–28.
[26] Baker AME, Windle AH. Polymer 2001;42:651–65.
[27] Müller A. Proc Roy Soc (London) 1932;A138:514–30.
[28] Swan PR. J Polym Sci 1962;56:403–7.
[29] Kobayashi Y, Keller A. Polymer 1970;11:114–7.
[30] Davis GT, Eby RK, Colson JP. J Appl Phys 1970;43:4316–26.
[31] Kavesh S, Schultz JM. J Polym Sci (A-2) 1970;8:243–76.
[32] Barham PJ, Keller A. J Mater Sci 1977;12:2141–8.
[33] Dadobaev G, Slutsker AI. Sov Phys Solid State 1981;23:1131–4.
[34] Fronk W, Wilke W. Coll Polym Sci 1981;259:797–807.
[35] Schauer K, Wilke W. Polymer Bull 1995;34:477–83.
[36] Pereira RA, Mano EB, Dias ML. Polymer Test 1997;16:589–601.
[37] Tashiro K, Ishino K, Ohta T. Polymer 1999;40:3469–78.
[38] Wang Z-G, Hsiao BS, Lopez J, Armistead JP. J Polym Res 1999;6:167–73.
[39] Slutsker AI, Vettegren VI, Gilyarov VL, Dodobaev G, Kulik VB, Titenkov LS. Polymer Sci Ser A 2002;44:729–34.
[40] Howard PR, Crist B. J Polym Sci Polym Phys Ed 1989;27:2269–82.
[41] Baker AME, Windle AH. Polymer 2001;42:681–98.
[42] Rabiej S. Eur Polym J 2005;41:393–402.
[43] Mitchell GR, Lovell R, Windle AH. Polymer 1982;23:1273–85.
[44] Seto T, Hara T, Tanaka K. Jpn J Appl Phys 1968;7:31–42.
[45] Bevis M, Crellin EB. Polymer 1971;12:666–84.
[46] Davis GT, Eby RK, Martin GM. J Appl Phys 1968;39:4973–81.
[47] Fischer EW, Goddar H, Schmidt GF. J Polym Sci (A-2) 1969;7:37–45.
[48] Davis GT, Weeks JJ, Martin GM, Eby RK. J Appl Phys 1974;45:4175–81.
[49] Hosoda S, Nomura H, Gotoh Y, Kihara H. Polymer 1990;31:1999–2005.
[50] Chen FC, Choy CL, Wong SP, Young K. J Polym Sci Polym Phys Ed 1981;19:971–81.
[51] Chen FC, Choy CL, Young K. J Polym Sci Polym Phys Ed 1980;18:2313–22.
[52] Vettegren VI, Slutsker AI, Gilyarov VL, Kulik VB, Titenkov LS. Phys Solid State 2003;45:1528–34.
[53] Hsie Y-L, Hu X-P. J Polym Sci B Polym Phys 1997;35:623–30.
[54] Goto M, Asada E. Bull Chem Soc Jpn 1978;51:2456–9.
[55] Kaneko F, Kobayashi M, Kitagawa Y, Matsuura Y. Acta Crystallogr 1990;C46:1490–2.
[56] Koetzle TF, Lehmann MS, Verbist JJ, Hamilton WC. Acta Crystallogr 1972;B28:3207–14.
[57] Brown GM, Levy HA. Science 1965;147:1038–9.
[58] Brown GM, Levy HA. Acta Crystallogr 1973;B29:790–7.
[59] Bunn CW. Trans Faraday Soc 1939;35:482–91.
[60] Kawaguchi A, Ohara M, Kobayashi K. J Macromol Sci Phys 1979;B16:193–212.
[61] Abrahamsson S, Dahlén B, Löfgren H, Pascher I. Prog Chem Fats Other Lipids 1978;16:125–43.
[62] Mo F, Hauback BC, Albon N. J Phys Chem 1993;97:6083–9.
[63] Iohara K-I, Imada K, Takayanagi M. Polym J 1972;3:357–64.
[64] Keith HD, Padden Jr FJ. J Appl Phys 1963;34:2409–21.
[65] Bassett DC. Principles of polymer morphology. Cambridge: Cambridge University Press; 1981.
[66] Abo el Maaty MI, Hosier IL, Bassett DC. Macromolecules 1998;31:153–7.
[67] Barham PJ, Keller A. J Polym Sci 1977;12:2141–8.